# SENSITIVITY OF PHASE DETECTION TECHNIQUES IN AERATED CHUTE FLOWS TO HYDRAULIC DESIGN PARAMETERS

**Daniel B. Bung** [1]

[1] Hydraulic Engineering Section, Department of Civil Engineering, FH Aachen University of Applied Sciences, Germany, Bayernallee 9, 52066 Aachen
E-mail: bung@fh-aachen.de

## Abstract

Flow properties in self-aerated high-speed flows are commonly investigated on large-scale hydraulic models with use of intrusive phase-detection probes. Digitalization of the raw voltage signals can be achieved by application of different techniques. User-defined thresholds need to be set which affect the resulting flow properties in different order. In this paper, three different techniques are applied with varying threshold settings to investigate effects on air content, flow resistance, energy dissipation and bubble count rate.

## Introduction

Investigation of air-water flow is one of the most challenging research fields in hydraulic engineering. This type of two-phase flow may occur on steep chutes, in hydraulic jumps, free plunging jets and breaking waves for instance.

As prototype measurements in regard to entrained air properties are difficult to conduct, large-scale laboratory studies are very common. According to Chanson (2002), the most reliable measuring technique for void fractions >10 % is given by intrusive needle probes, which may be based on optical or conductivity principles (Fig. 1a and 1b). Phase changes detection is achieved as bubbles are pierced by the needle tips with diameters of ~100 µm. Depending on the surrounding medium (i.e. water or air), a low or high voltage raw signal is recorded which needs to be digitalized in order to characterize air properties, such as total air concentration, air bubble sizes and velocities.

A typical raw signal measured with a conductivity probe in a high-speed self-aerated spillway flow is given in Fig. 2a. Note that the transition from water to air is characterized by a low gradient, the transition from air to water by a high gradient, due to wetting and drying of the probe tip (Toombes, 2002). Cartellier (1992) and Cummings (1996) declare the tangent points A and B to correspond to the passage of the rear and front bubble interface on the probe and thus, to the physical phase changes.

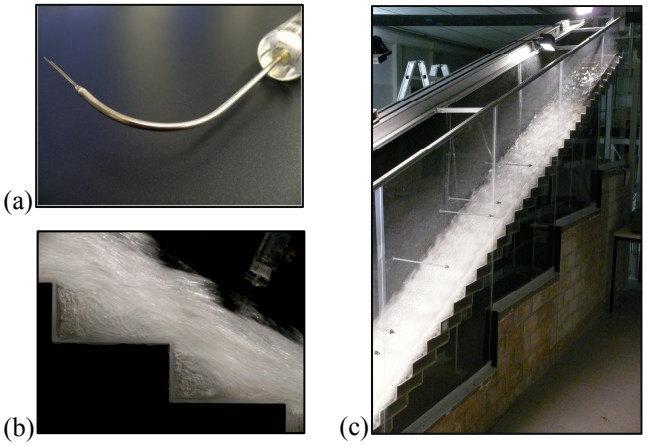


Figure 1: Experimental setup, (a): conductivity probe for detection of void fraction (here: double-tip probe allowing velocity measurements), (b): experiment in aerated stepped spillway flow, (c): overview of total model setup for stepped spillway configuration

In order to interpret the data in regard to air-water flow properties, the signal is commonly digitalized to a well-defined square wave signal. Three digitalization techniques are widely-used:

1. Single threshold technique (ST): A single threshold voltage between user-defined, representative voltages for air and water phase is defined. Samples below this threshold are assumed to be measured in air, higher samples to be measured in water.
1. Double threshold technique (DT): Two threshold voltages are set, one lower than the representative water voltage $U_w$ and one higher than the air voltage $U_a$, thresholds are closer to real phase transition.
2. Combined double threshold and slope technique (DTS): Additional slope criterion demanding a minimum slope near the tangent points A and B.

According to Chanson and Carosi (2007) the ST technique is a robust digitalization method for free-surface flows. Toombes (2002) and Chanson and Felder (2010) choose a threshold of 50 % of the air-water range $\Delta U = U_w - U_a$ for stepped spillway flows. According to Chanson and Felder (2010), a threshold variation between 25 % and 85 % has only little effect on the resulting void fraction.

By use of the DT technique (e.g., Boes 2000, Kramer 2004), thresholds are set closer to the physical phase transition points A and B (Fig. 2b). Kramer (2004) states that the resulting air concentration is more influenced by a variation of the upper threshold leading to deviations up to 10 %. However, the possibility of misinterpreting spurious bubbles due to noise is increasing (Toombes, 2002). In order to ignore these small spikes in this study, phase change is only assumed if the signal passes both thresholds. Alternatively, the DTS technique may be applied which additionally implies a slope criterion demanding a minimum slope of the signal in the vicinity of the phase change points (e.g., Cummings 1996, Thorwarth 2008, Bung 2009).

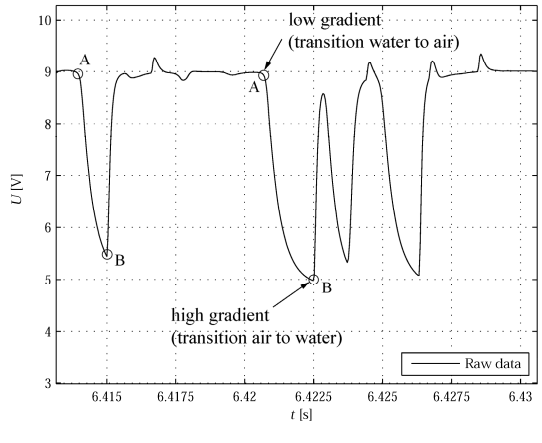


(a)

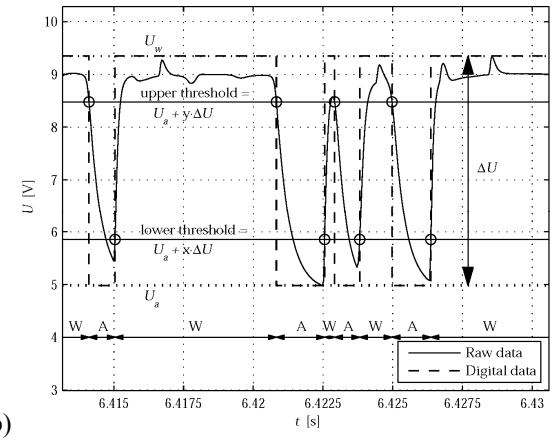


(b)

Figure 2: Raw data sampled with a conductivity probe, (a): phase transition gradients and tangent points A and B, (b): double-threshold digitalization (DT) with exemplary user-defined parameters $x$ and $y$

All digitalization techniques are based on different user-defined and thus, subjective parameter settings. In this study, the sensitivity of applied digitalization methods and parameter settings on resulting air-water flow properties is analyzed. For this purpose, raw data gathered on moderately sloped chute models with $\phi = 26.6°$ is taken into account. On the one hand, a smooth invert chute is investigated. On the other hand, data sampled on a stepped spillway model with 6 cm steps height is observed for comparison (Fig. 1b). It should be noted that the bottom of the smooth invert chute model is equipped with an artificial roughness to enhance the aeration process in the laboratory. Scaling to prototype dimensions is unfeasible, but qualitative flow characteristics are unaffected.

## Experimental setup and methodology

Experiments are conducted on a spillway model 2.34 m high and 0.30 m wide (Fig. 1c). By investigating three specific discharges (i.e., $q$ = 0.07 m²/s, $q$ = 0.09 m²/s and $q$ = 0.11 m²/s), skimming flow regime sets in on the stepped spillway model with step height $s$ = 6 cm and uniform flow conditions are found to set in for both model configurations (i.e., the smooth invert chute and the stepped spillway).

In this study, air-water flow properties are measured by means of a double-tip conductivity probe (manufactured at IWW, RWTH Aachen, Fig. 1a). This probe is characterized by two electrodes which are arranged back-to-back in flow direction and allow the determination of flow velocity by cross-correlating both signals. Probe tips are 130 µm thin. Raw signals are recorded for 25 s with a sample rate of 25 kHz. Exact probe positioning is achieved by a two-dimensional linear guide system operated by a CNC controller (isel). Measurements are carried out in the centerline of the flume (at step edges for the stepped spillway). Data analysis will be limited to the uniform flow region. Digitalization is performed by above-mentioned techniques with parameter settings given in Tab. 1:

Table 1: Threshold combinations (in percentage of $\Delta U$) for different digitalization methods

| ST | DT | DTS |
|---|---|---|
| 0.20 | 0.10/0.80 | |
| 0.35 | 0.10/0.90 | |
| 0.50 | 0.20/0.80 | 0.20/0.80 |
| 0.65 | 0.20/0.90 | |
| 0.80 | 0.30/0.70 | |

## Results

### General

As mentioned above, characteristic voltages $U_a$ for air and $U_w$ for water, respectively, need to be defined for all digitalization techniques. In this study, the 0.02$^{th}$ and 99.8$^{th}$ percentiles are chosen (i.e. 0.02/99.8 % of the measuring

values are lower) and a variation is not carried out. The minimum slope near the phase transition tangent points for DTS is defined as the $10^{th}/90^{th}$ percentile of detected slopes during a sample.

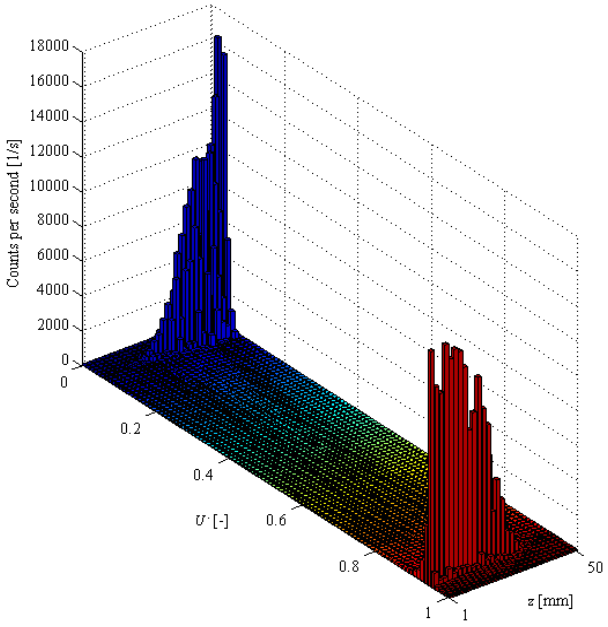


(a)

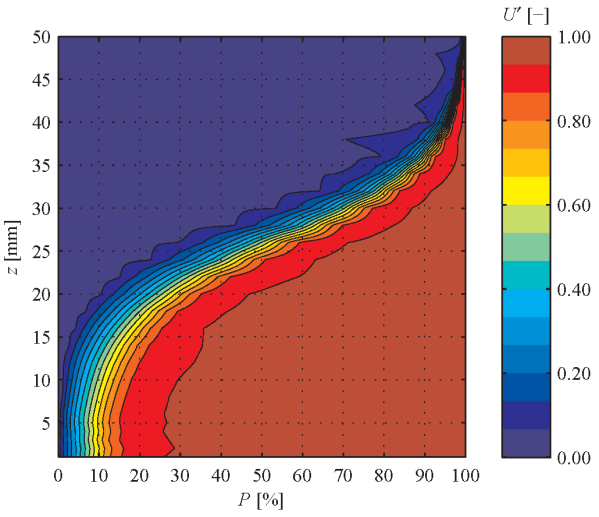


(b)

Figure 3: Typical raw signal characteristics, exemplarily for the smooth invert chute model with $q$ = 0.07 m²/s, (a) dimensionless voltage histogram (in counts per second), (b) dimensionless voltage probability distribution

Typically, the voltage signal in lower flow depths $z$ consists of high values as this region is characterized by single air bubbles and pockets surrounded by a continuous water phase (i.e. the bubbly flow region, Chanson 1995). Near the air-water surface, the mixture consists of water droplets flowing in an air flow (Chanson 1995) and leading to a majority of low voltage values. An exemplary voltage histogram is illustrated in Fig. 3(a). Please note that the illustration includes a dimensionless voltage $U'$ ($0 \le U' \le 1$) defined as

$$U' = \frac{U - \min(U)}{\max\left(U - \min(U)\right)} \quad (1)$$

where $U$ is the originally measured voltage (in Hz). Figure 3b shows the related probability distribution. Obviously, the signal values are more spreading in lower flow depths, with increasing flow depths the probability distribution curves narrow and thus, indicate that $U'$ is more likely equal to 0 or 1 than near the bottom. By consequence, it can be assumed that the digitalization is more accurate for low $z$.

**Air concentration**

The air concentration detected by each digitalization technique is defined as

$$C = \frac{\sum t_{air}}{t_{sample}} \quad (2)$$

where $t_{air}$ is the duration where the digitalized square wave signal equals the characteristic air voltage and $t_{sample}$ is the total sample time.

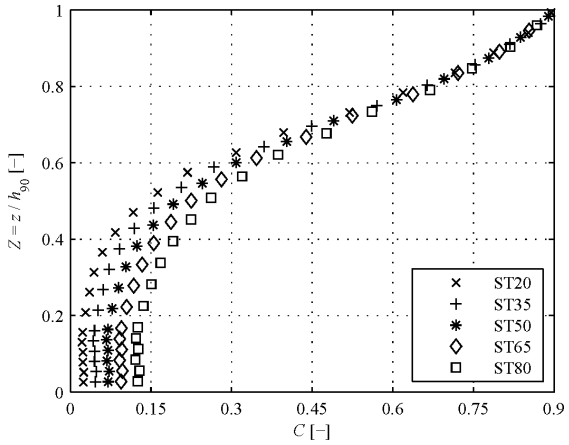


(a)

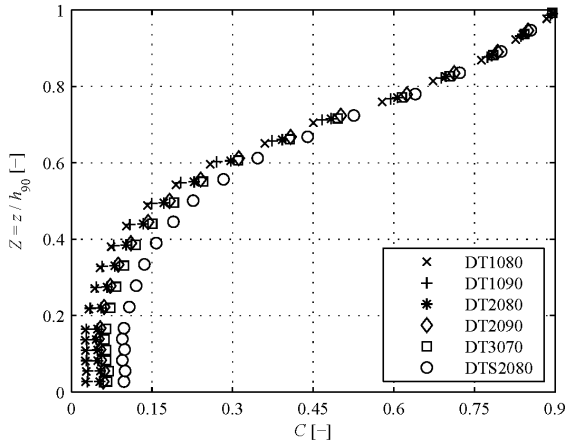


(b)

Figure 4: Dimensionless air concentration profiles for different thresholds, exemplarily for the smooth invert chute model with $q$ = 0.07 m²/s, (a) ST method, (b) DT/DTS method

Figure 4 exemplarily presents typical air concentration distributions obtained for $q$ = 0.07 m²/s on the smooth invert chute model by both, the ST and DT method, with threshold settings according to Tab. 1. Obviously, the detected void fraction is affected by threshold variation, particularly for $C$ < 40 %, i.e. the bubbly flow region according to Chanson (1995). It should be noted that the air concentration $C$ is plotted versus the dimensionless water depth $Z = z / h_{90}$, where $h_{90}$ is the water depth with $C$ = 90 % ($h_{90} \approx$ 36 mm for all digitalization techniques in Fig. 4). While the sensitivity is less for DT method, threshold variation leads to different bottom air concentrations between 2.4 % and 12.6 % for the ST method. In regard to the cavitation risk on the structure, this parameter is of major importance. Similar results are found for the other investigated discharges and on the stepped spillway model. Resulting depth-averaged mean air concentrations

$$\overline{C} = \frac{1}{h_{90}} \int_{z=0}^{z=h_{90}} C(z)\,\mathrm{d}z \qquad (3)$$

as well as bottom air concentration $C_b$ for all model tests are listed in Tab. 2 and 3. Both parameters are increasing with increasing threshold for ST method or with increasing lower threshold for DT method. The upper threshold for DT technique is of minor influence.

The DTS method (here with thresholds of 20 and 80 % of $\Delta U$) which is theoretically the most accurate technique as the tangent points are best represented by the digital signal and spurious phase changes are neglected due to the gradient criterion, compares well to ST65. In regard to determination of air concentration, calculation time may be reduced in the order of 50 % by use of the latter.

Table 2: Mean air contents $\overline{C}$ for all configurations (values for $s$ = 0 cm not to be scaled due to artificial bottom roughness)

| | **$s$ = 0 cm** | | | **$s$ = 6 cm** | | |
|---|---|---|---|---|---|---|
| ***q* [m²/s]** | **0.07** | **0.09** | **0.11** | **0.07** | **0.09** | **0.11** |
| **ST20** | 0.292 | 0.268 | 0.259 | 0.287 | 0.278 | 0.264 |
| **ST35** | 0.311 | 0.285 | 0.274 | 0.311 | 0.294 | 0.277 |
| **ST50** | 0.330 | 0.304 | 0.288 | 0.332 | 0.313 | 0.291 |
| **ST65** | 0.347 | 0.323 | 0.307 | 0.350 | 0.331 | 0.312 |
| **ST80** | 0.370 | 0.347 | 0.329 | 0.367 | 0.352 | 0.335 |
| **DT1080** | 0.300 | 0.272 | 0.260 | 0.295 | 0.278 | 0.261 |
| **DT1090** | 0.298 | 0.274 | 0.260 | 0.298 | 0.280 | 0.264 |
| **DT2080** | 0.313 | 0.287 | 0.273 | 0.318 | 0.297 | 0.277 |
| **DT2090** | 0.317 | 0.291 | 0.277 | 0.321 | 0.301 | 0.282 |
| **DT3070** | 0.325 | 0.299 | 0.283 | 0.330 | 0.308 | 0.288 |
| **DTS2080** | 0.349 | 0.325 | 0.309 | 0.347 | 0.332 | 0.313 |
| ***P(U'*≤0.5)** | 0.328 | 0.303 | 0.287 | 0.375 | 0.312 | 0.291 |

Table 3: Bottom air concentrations $C_b$ for all configurations (values for $s$ = 0 cm not to be scaled due to artificial bottom roughness)

| | **$s$ = 0 cm** | | | **$s$ = 6 cm** | | |
|---|---|---|---|---|---|---|
| ***q* [m²/s]** | **0.07** | **0.09** | **0.11** | **0.07** | **0.09** | **0.11** |
| **ST20** | 0.024 | 0.010 | 0.008 | 0.009 | 0.010 | 0.006 |
| **ST35** | 0.047 | 0.023 | 0.019 | 0.021 | 0.024 | 0.015 |
| **ST50** | 0.070 | 0.041 | 0.035 | 0.034 | 0.041 | 0.026 |
| **ST65** | 0.095 | 0.063 | 0.057 | 0.049 | 0.059 | 0.040 |
| **ST80** | 0.126 | 0.092 | 0.086 | 0.068 | 0.084 | 0.061 |
| **DT1080** | 0.027 | 0.012 | 0.008 | 0.011 | 0.011 | 0.008 |
| **DT1090** | 0.029 | 0.013 | 0.009 | 0.013 | 0.012 | 0.010 |
| **DT2080** | 0.053 | 0.024 | 0.020 | 0.025 | 0.027 | 0.017 |
| **DT2090** | 0.059 | 0.027 | 0.022 | 0.029 | 0.032 | 0.021 |
| **DT3070** | 0.067 | 0.035 | 0.030 | 0.032 | 0.037 | 0.024 |
| **DTS2080** | 0.098 | 0.066 | 0.061 | 0.051 | 0.062 | 0.043 |
| ***P(U'*≤0.5)** | 0.071 | 0.041 | 0.036 | 0.034 | 0.040 | 0.025 |

When comparing Figs. 3 and 4, it can be seen that the probability distribution curves of dimensionless voltages have a similar shape as typical air concentration profiles. Sensitivity of threshold parameters is higher in bubbly flow region where voltage values are more scattered. However, it is found that the probability distribution curve for $U' \leq 0.5$ represents well the air concentration profile obtained by ST50 method when the probability $P$ is assumed as the air content $C$. Resulting mean air contents and bottom air concentrations are given in Tab. 2 and 3 as well indicating that results compare well except for the stepped spillway model with $q$ = 0.07 m²/s. The deviation for this configuration is probably due to the present flow regime (i.e. the transition flow regime occurring for low $h_c/s$, where $h_c$ is the critical water depth) involving a more chaotic flow pattern (Ohtsu and Yasuda 1997, Chanson and Toombes 2001).

**Flow resistance and residual energy**

The Darcy friction factor in uniform flow region may be determined by

$$f = \frac{8g \sin\phi h_w^3}{q^2} \qquad (4)$$

where $g$ is the acceleration due to gravity, $h_w = h_{90}(1-\overline{C})$ the clear water depth and $q$ the specific discharge. As the characteristic air-water mixture depth $h_{90}$ was found to be unaffected by the digitalization method, the flow resistance is directly influenced by mean air content deviations according to Tab. 2. Consequently, the flow resistance is decreasing with increasing threshold for ST method and increasing lower threshold for DT method. Resulting friction factors are listed in Tab. 4.

Table 4: Friction factors $f$ for all configurations (values for $s$ = 0 cm not to be scaled due to artificial bottom roughness, min. and max. values for both spillways underlined)

| | $s$ = 0 cm | | | $s$ = 6 cm | | |
|---|---|---|---|---|---|---|
| $q$ [m²/s] | **0.07** | **0.09** | **0.11** | **0.07** | **0.09** | **0.11** |
| **ST20** | 0.121 | 0.139 | 0.122 | 0.230 | 0.195 | 0.202 |
| **ST35** | 0.104 | 0.122 | 0.107 | 0.198 | 0.168 | 0.177 |
| **ST50** | 0.091 | 0.107 | 0.095 | 0.173 | 0.147 | 0.157 |
| **ST65** | 0.080 | 0.094 | 0.085 | 0.152 | 0.130 | 0.140 |
| **ST80** | 0.069 | 0.081 | 0.073 | 0.131 | 0.112 | 0.122 |
| **DT1080** | 0.107 | 0.124 | 0.108 | 0.206 | 0.173 | 0.179 |
| **DT1090** | 0.103 | 0.120 | 0.104 | 0.199 | 0.167 | 0.173 |
| **DT2080** | 0.096 | 0.112 | 0.099 | 0.182 | 0.155 | 0.164 |
| **DT2090** | 0.091 | 0.108 | 0.095 | 0.173 | 0.148 | 0.158 |
| **DT3070** | 0.091 | 0.107 | 0.095 | 0.171 | 0.147 | 0.157 |
| **DTS2080** | 0.080 | 0.093 | 0.084 | 0.150 | 0.129 | 0.139 |
| ***P(U'*≤0.5)** | 0.086 | 0.102 | 0.092 | 0.133 | 0.140 | 0.151 |

The Darcy friction factor is directly related to the energy dissipation potential of the structure. For a free inflow condition with critical flow conditions at the crest, it yields (neglecting the velocity head correction factor valid for fully turbulent flows):

$$\frac{H_{res}}{H_{\max}} = \frac{\left(\frac{f}{8\sin\phi}\right)^{1/3}\cos\phi + \frac{1}{2}\left(\frac{f}{8\sin\phi}\right)^{-2/3}}{1.5 + \frac{H_{dam}}{h_c}} \quad (5)$$

where $H_{res}$ is the residual energy head at the spillway toe, $H_{max}$ is the maximum energy head ($H_{max} = H_{dam} + 1.5h_c$) and $H_{dam}$ is the crest height above ground.

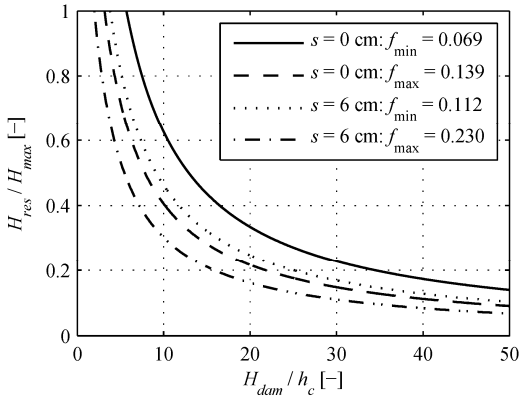


Figure 5: Dimensionless residual energy heads $H_{res} / H_{max}$ as a function of the relative dam height $H_{dam} / h_c$ for min. and max. friction factors $f$ determined for both spillways (Tab. 4)

Residual energy head curves for both spillways on basis of minimum and maximum friction factors (underlined in Tab. 4) are illustrated in Fig. 5. Although $f$ was found to be doubled by application of different digitalization methods, the effect on the residual energy head, which is important for hydraulic engineering purposes, is small (particularly for high structures with $H_{dam} / h_c > 10$).

**Bubble count rate**

The bubble count rate $F_B$ is defined as the number of detected air bubbles per second. When measured in laboratory, scale effects generally have to be taken into account due to similar bubble sizes in laboratory and nature. Besides being directly related to the present air-water interface which is important for gas exchange processes (Chanson 1995, Schlenkhoff and Bung 2009, Bung 2011), $F_B$ may be used for determination of turbulence intensity (Chanson and Felder 2010).

It is known that the bubble count rate $F_B$ follows a parabolic distribution when plotted against air concentration $C$, with its maximum $F_{B,max}$ at $C$ ~50 % (Chanson and Toombes 2001, Toombes 2002).

Fig. 6 shows the bubble count rate distributions for $s$ = 0 cm and $q$ = 0.07 m²/s determined on basis of the different digitalization methods. Maximum bubble count rates for all configurations are listed in Tab. 5. It is found that $F_B$ is significantly affected by the threshold settings as well as by the method itself. For both, the ST and the DT technique, deviations in the order of 100 % are found for varying thresholds. Moreover, the DT method detects only approximately half of the bubble counts (max. ~61 to 131 Hz) found by the ST method (max. ~100 to 251 Hz). The highest absolute deviations are found for $F_{B,max}$ ($C$ ~40 %), i.e. the region where the air concentration becomes unaffected by the digitalization method. The DTS technique results in similar bubble counts as ST65 and ST80. When the ST method is applied, a minimum threshold is found from where $F_B$ remains almost constant (65 % of $\Delta U$ in Fig. 6a). Similar results are presented by Chanson and Felder (2011).

Table 5: Maximum bubble count rates $F_{B,max}$

| | $s$ = 0 cm | | | $s$ = 6 cm | | |
|---|---|---|---|---|---|---|
| $q$ [m²/s] | **0.07** | **0.09** | **0.11** | **0.07** | **0.09** | **0.11** |
| **ST20** | 100 | 115 | 126 | 115 | 115 | 123 |
| **ST35** | 138 | 154 | 163 | 161 | 153 | 155 |
| **ST50** | 181 | 198 | 206 | 198 | 200 | 199 |
| **ST65** | 206 | 228 | 239 | 222 | 227 | 232 |
| **ST80** | 216 | 241 | 251 | 232 | 235 | 246 |
| **DT1080** | 65 | 70 | 75 | 62 | 66 | 74 |
| **DT1090** | 61 | 65 | 70 | 58 | 61 | 68 |
| **DT2080** | 86 | 92 | 99 | 88 | 89 | 95 |
| **DT2090** | 79 | 85 | 90 | 81 | 82 | 86 |
| **DT3070** | 114 | 123 | 131 | 127 | 123 | 123 |
| **DTS2080** | 219 | 244 | 258 | 241 | 244 | 251 |

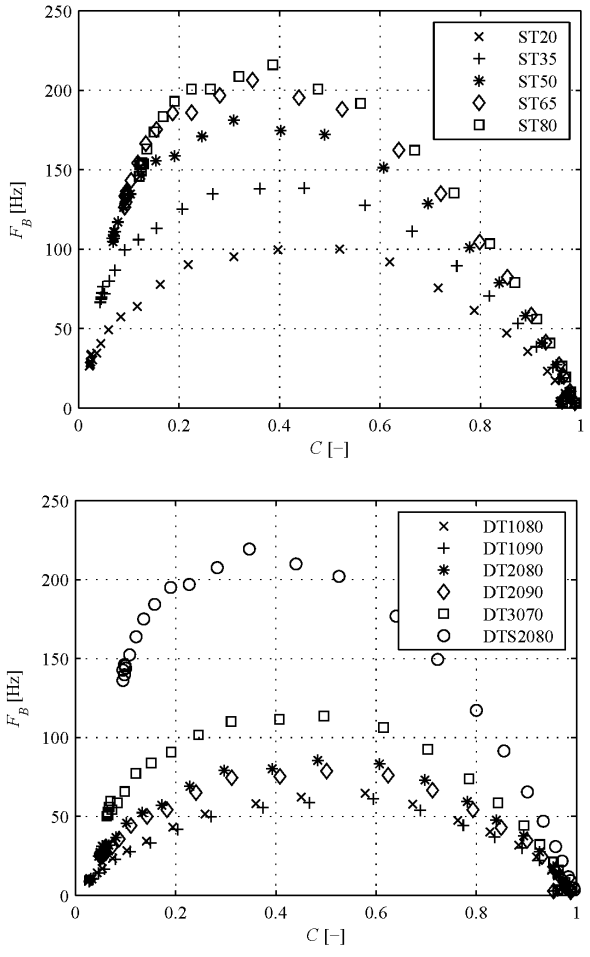


Figure 6: Bubble count rates $F_B$ for different thresholds, exemplarily for the smooth invert chute model with $q$ = 0.07 m²/s, (a) ST method, (b) DT/DTS method

## Conclusion

A comprehensive study on digitalization techniques for air-water flow raw signals was presented. Therefore, model tests were conducted on a smooth invert chute model and a stepped spillway model. Besides the simple single threshold method, two double threshold methods were applied (namely the basic double threshold method and the same with an additional slope criterion).

It was found that the method as well as the threshold settings have different influence on different flow parameters. While the air concentration is particularly sensitive in the bubbly flow region close to the bottom, the bubble count rate is mostly affected in the flow depth where $C$ is ~40 %.

Assuming that the DTS method is the most accurate as the tangent point of phase changes are best approximated and spurious bubbles are neglected due to the slope criterion, the ST65 configuration is found to yield equivalent results. Hence, the calculation time can be significantly reduced without loss of accuracy when applying this single threshold method. A higher threshold results in higher air concentration and bubble count rate as more spurious bubbles are considered which are generated by signal noise in high-voltage regions as can be seen in Fig. 2. Consequently, a lower flow resistance is derived.

The DT method leads to a significant underestimation of bubble count rates. This may be due to the underlying criterion applied in this study that both, the upper and lower threshold, need to be crossed for interpretation as a phase change.

Furthermore, it was found that the void fraction can be directly estimated from the probability distribution of the raw signals taking into account the minimum and maximum detected voltage only. Thus, a time consuming digitalization as well as the definition of a characteristic air voltage and water voltage, respectively, become dispensable when focusing on air concentration only. Here, a more detailed future investigation on statistical relationships of raw data values is needed.

## References


Boes, R.M. (2000). *Zweiphasenströmung und Energieumsetzung an Großkaskaden*. PhD thesis, ETH Zurich (in German).

Bung, D.B. (2011). *Fließcharakteristik und Sauerstoffeintrag bei selbstbelüfteten Gerinneströmungen auf Kaskaden mit gemäßigter Neigung*. ÖWAW 3-4/2011, pp. 76-81 (in German).

Cartellier, A. (1992). *Simultaneous void fraction measurement, bubble velocity, and size estimate using a single optical probe in gas-liquid two-phase flow*. Rev. Sci. Instrum. 63(11), pp. 5442-5453.

Chanson, H. (1995). *Predicting Oxygen Content Downstream of Weirs, Spillways and Waterways*. Proc. Instn Civ. Engrs Wat. Marit. & Energy, Vol. 112, pp. 20-30.

Chanson, H. (2002). *Air-Water Flow Measurements with Intrusive, Phase-Detection Probes: Can We Improve Their Interpretation?* J. Hydr. Eng. 128(3), pp. 252-255.

Chanson, H. , Carosi, G. (2007). *Advanced Post-Processing and Correlation Analyses in High-Velocity Air-Water Flows*. Env. Fluid Mech. 7(6), 495-508.

Chanson, H., Felder, S. (2010). *Turbulence Measurements in Air-Water Self-Aerated Flows: Basic Analysis and Results*. Proc. 7th Int. Conf. on Multiphase Flows, Tampa.

Chanson, H., Toombes, L. (2001). *Experimental investigations of air entrainment in transition and skimming flows down a stepped chute*. Tech. Rep. CE158. University of Queensland.

Cummings, P.D. (1996). *Aeration due to Breaking Waves*. PhD thesis, University of Queensland.

Kramer, K. (2004). *Development of Aerated Chute Flow*. PhD thesis, ETH Zurich.

Ohtsu, I., Yasuda, Y. (1997). Characteristics of flow conditions on stepped spillways. 27th IAHR Congress. San Francisco, 583-588.

Schlenkhoff, A., Bung, D.B. (2009): *Prediction of oxygen transfer in self-aerated skimming flow on embankment stepped spillways*. Proc., 33rd IAHR Congress, IAHR, Vancouver.

Thorwarth, J. (2008). *Hydraulisches Verhalten von Treppengerinnen mit eingetieften Stufen - Selbstinduzierte Abflussinstationaritäten und Energiedissipation*. PhD thesis, RWTH Aachen (in German).

Toombes, L. (2002). *Experimental Study of Air-Water Flow Properties on Low-Gradient Stepped Cascades*. PhD thesis, University of Queensland.